Supplementary Materials and Methods

EMS mutagenesis

Over 3000 *Arabidopsis* seeds were surface sterilized with ethanol 95% (v/v) ethanol for 10min and 20% (v/v) bleach for 6 min. The sterilized seeds were left overnight at 4°C on a rocker in distilled water. Then seeds were incubated with 0.04% EMS (SIGMA-M0880) during in 100 mM sodium phosphate buffer, pH 7. After 9 hours the seeds were washed ten times with distilled water to remove EMS residues. EMS mutagenized seeds (M1) were propagated under greenhouse conditions and F1 seeds (M2) were harvested and grown under -Pi conditions. Mutants that presented a long-root phenotype under in -Pi media were selected.

Transcriptional reporter lines

4900pb (stop1Fw:GAACGACAAGATTACAAGTAGGTTC and stop1Rv:GTTGCACAAATCGTCTTCAGTTTCC) and 2253 (almt1Fw:GGCAGATAAAGAGGCACTCGTG and almt1Rv:CTCTCTCACTTTCTCCATAACACC) intergenic region lengths were used to build the *proSTOP1::GUS-GFP* and *proALMT1::GUS-GFP* transcriptional reporter lines respectively. Intergenic region were cloned on the pKGWFS7,0 using the Gateway system. *Arabidopsis* plants were agro-infiltrated using the floral-dip method (1).

Histochemical GUS staining

Histochemical GUS staining was performed as reported by (2). The stained roots were clarified following the protocol reported by (3). A representative root stained was chosen and photographed using Nomarski optics on a Leica DMR microscope.

Malate and Fe2+, Fe3+ and Al3+ Molecular Dynamics

Molecular dynamic (MD) calculations were carried out to obtain insight about the behavior between malate molecules and Fe(II), Fe(III), Al(III) ions in explicit water solution. Non-bonded parameters for the metallic cations were taken from the 12-6-4 Lennard-Jones-type non-bonded model for divalent (4) and highly charged metal ions (5) respectively. These parameters were then adapted to the GROMOS 53a6 force field and integrated with GROMACS 5.0 as a user specified non-bonded potential employing tabulated interaction functions (6). The all-atom PDB optimized geometry structure and parameters for malate molecules were taken from the ATB web server (7). A total of nine systems were built with the malate-Fe(II), malate-Fe(III) and malate-Al(III) proportions of 0:120, 40:120, 80:120 and 120:120 within a cubic box with periodic boundary conditions. In all systems, the box was solvated with SPC/E (8) type water molecules and the steepest descents method was employed to minimize the energy. The temperature was set to 300 K and an equilibration phase of 100 ps in the canonical ensemble (NVT) was conducted using the V-rescale algorithm (9). Long-range electrostatics were calculated employing the PME method (10), 11) with a cutoff of 12 Å and the same cutoff was chosen for the van der Walls non-bonded interactions. All bond lengths were constrained with Linear Constraint Solver (LINCS; (12). A final production of 50 ns in the isothermal-isobaric ensemble (NPT) was conducted using the Parrinello-Rahman algorithm (13). Snapshots were stored after each 10 ps and the final MD trajectories were analyzed using the g_aggregate tool (14).

Preparation of root tip mRNA-seq libraries

Total RNA was isolated from frozen root tip powder using TRIzol reagent (Invitrogen) according to the manufacturer's instructions. Frozen root tip powder was obtained from

root tip sections of approximately 2-3 mm length from approximately 500 individuals per treatment (5 dag). Non-strand specific mRNA-seq libraries were generated from 5 µg of total RNA and prepared using the TruSeq RNA Sample Prep kit (Illumina) according to the manufacturer's instructions.

RNA-seq High-throughput Sequencing and Data Analysis

Quality assessment of the reads generated with the Illumina analysis pipeline (fastq format) was performed using FastQC (version 0.11.4) and processed using Trimmomatic (15) (version 0.35) to remove reads that contained adapter sequences and low quality reads. Single and paired-end clean reads were aligned to the Arabidopsis thaliana TAIR10 reference sequence using TopHat2 (16) (version 2.0.9). Raw counts per gene were estimated using HTseq (17) (version 0.6.0). Data was normalized in edgeR (18) (version 3.12.0) using the trimmed mean of M values (TMM) method. Genes with ≥ 3 reads in total, across all samples, were included in the final analysis. Transcript abundance as represented by the normalized raw counts per gene was used to determine differential expression using the edgeR package. Analysis of GO enriched categories and clusterization into functional groups by biological process was performed using Cytoscape (19) (version 3.4) plugin ClueGO+CluePedia (20).

Genomic data generated in this study is accessible at www.ncbi.nlm.nih.gov/biosample/
Accession codes:
WT-*lpi5*: SAMN05991845; Mutant-*lpi5*: SAMN05991846; WT-*lpi6*: SAMN05991847; Mutant-*lpi6*: SAMN05991848;
http://www.ncbi.nlm.nih.gov/biosample/5991845
http://www.ncbi.nlm.nih.gov/biosample/5991846
http://www.ncbi.nlm.nih.gov/biosample/5991847
http://www.ncbi.nlm.nih.gov/biosample/5991848

Expression data generated in this study is deposited in the Gene Expression Omnibus database (GSE90061) and can be accessed at:
https://www.ncbi.nlm.nih.gov/geo/

Supplementary Figures

Cross	*F1 progeny* Phenotypes		*F2 progeny* Phenotype observed		Ration obtained		Ration tested		
	WT	mutant	WT	mutant	WT	mutant	WT	mutant	X^{2*}
lpi5 x Col-0	179	0	490	170	2.97	1.03	3	1	0.2
lpi6 x Col-0	148	0	577	182	3.04	0.96			0.42
							[a]95%		3.841

* With one degree of freedom and a critical value of 5% we fail to reject the hypothesis of a Mendelian ratio of segregation (3:1, WT:mutant) if the x^2 is smaller than 3.841.

Supplementary Table 1. Segregation ratios of the F2 progeny seedlings obtained from *lpi5* X WT and *lpi6* X WT crosses.

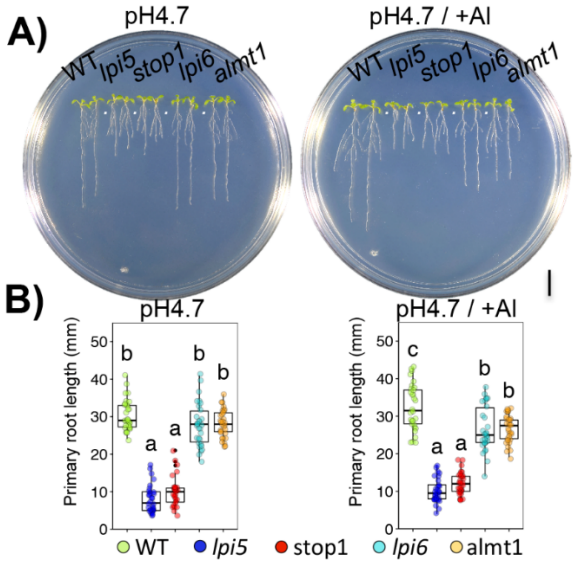

C Segregation ratios

	Phenotype of F1-population	
	Col-0	Mutant
stop1 vs lpi5	0	120
almt1 vs lpi6	0	82

Supplementary Figure 1. **Primary root growth of *lpi5*, *stop1*, *lpi6* and *almt1* 10-day-old seedlings in response to low pH and aluminum toxicity.** (A) Boxplot representation of the primary root length of WT, *lpi5, stop1, lpi6,* and *almt1* 10-day-old individuals (n=30) grown under low pH (4.6) (left) and aluminum toxicity (2 µM) (right) conditions. Dots represent individuals and genetic backgrounds are depicted by colors as described. Statistical groups were determined using a Tukey HSD test (P-value < .05) and are indicated by a letter. B) WT, *lpi5, stop1, lpi6,* and *almt1* 10-dag seedlings grown under low pH (4.6) (left) and aluminum toxicity (2 µM) (right) conditions.

Scale bar equals 1 mm. C) Segregation ratios of F1 progeny seedlings (long root phenotype under -Pi conditions) obtained from *stop1* vs *lpi5* and *almt1* vs *lpi6* crosses. All F1 progeny seedlings from the *lpi5* x *salk_114108* and *lpi6* x *salk_009629* crosses were observed to have a mutant phenotype under –Pi conditions.

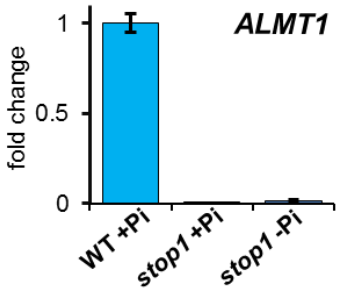

Supplementary Figure 2. ***STOP1* is essential for *ALMT1* expression in the root tip.** qRT-PCR analysis of *ALMT1* expression in root apex of WT and *stop1* plants. Bars represent the mean logFC ±SEM of 2 biological replicates with 3 technical replicates. WT +Pi samples were used as calibrator values. *ACT2* and *UBQ10* were used as internal controls.

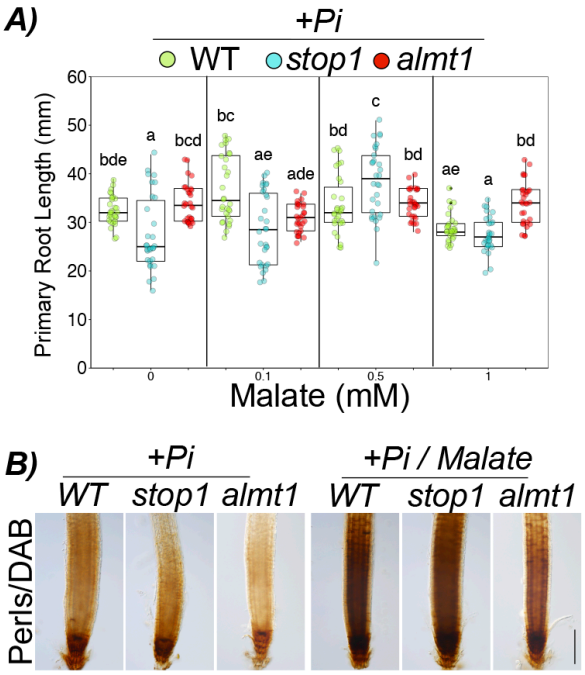

Supplementary Figure 3. Malate effect on primary root growth and iron distribution in the root under high phosphate conditions. (A) Primary root length of 10 dag WT, *stop1* and *almt1* seedlings in response to increasing concentrations of malate supplemented to +Pi medium. (B)

DAB-Perls iron staining of roots from 10 dag WT, *stop1* and *almt1* seedlings grown under +Pi and +Pi medium supplemented with 1 mM malate (+Pi+M).

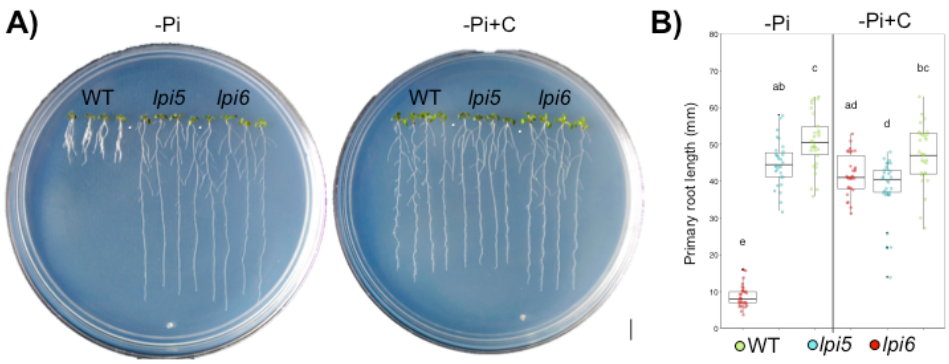

Supplementary Figure 4. Citrate supplementation of low Pi medium did not rescue the long root phenotype of *stop1 and almt1* mutants. (A) Phenotypes of 10 dag WT, *stop1* and *almt1* seedlings grown in low phosphate medium (-Pi) and low phosphate medium supplemented with 1mM citrate (-Pi+C). Scale bar equals 1 mm. (B) Primary root length of 10 dag WT, *stop1* and *almt1* seedlings under -Pi and -Pi medium supplemented with 1mM citrate. Green, blue and red dots depict WT, *stop1* and *almt1* individuals (n=30 from 3 independent experiments), respectively. Statistical groups were determined using Tukey HSD test (P-value <.05) are indicated with letters.

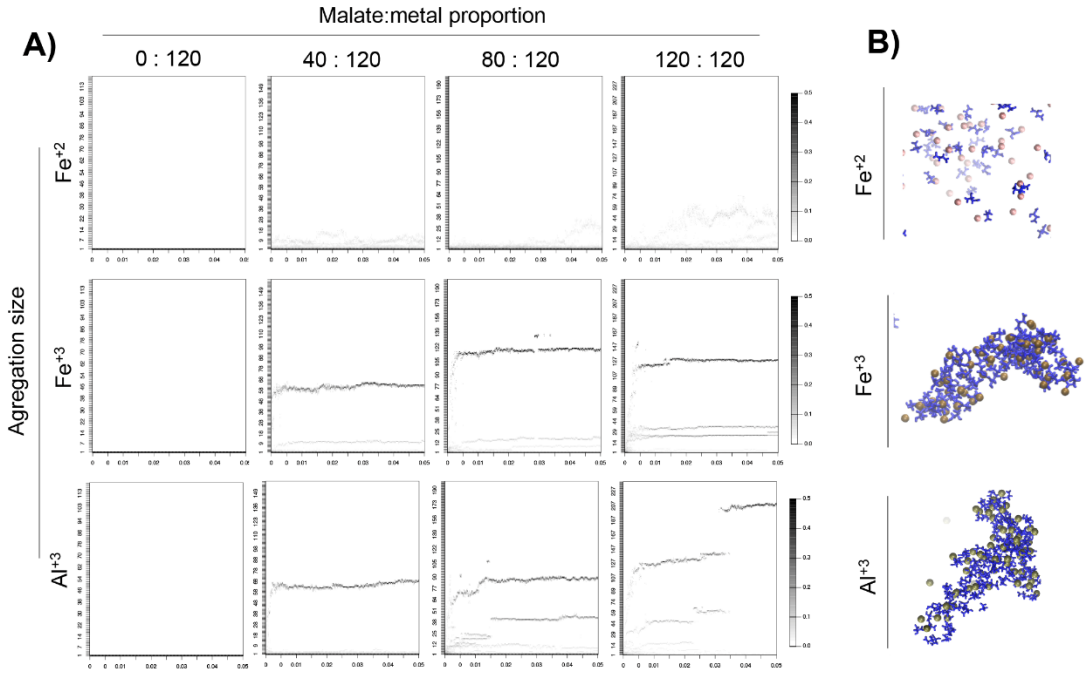

Supplementary Figure 5. Molecular dynamic calculations revealed the malate-chelating effect that induces Fe^{+3} aggregation. 120 molecules of each metal (A-D) Fe^{+2}, (E-H) Fe^{+3} and (I-

L) was simulated (see Materials and Methods) with 0, 40, 80 and 100 molecules of malate, respectively. Structural representation at the end (50 microseconds) of simulation between the higher malate concentration (120 molecules) and (M) Fe^{+2}, (N) Fe^{+3} and (O) Al^{+3}, respectively.

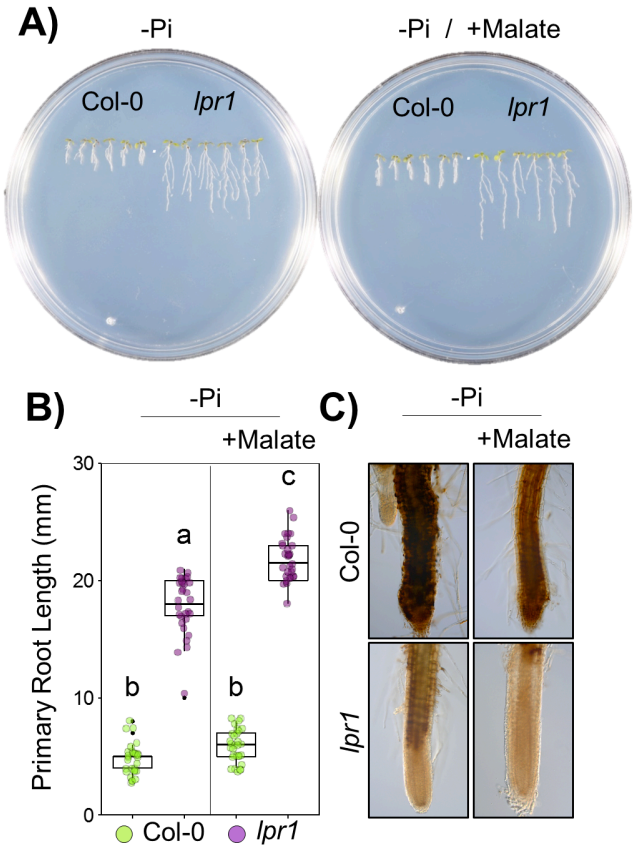

Supplementary Figure 6. Malate supplementation of low Pi medium did not rescue the long root phenotype of *lpr1* mutants. (A) Phenotypes of Col-0 (WT) and *lpr1* seedlings grown under -Pi conditions (left) and -Pi medium supplemented with 1 mM malate (-Pi+M) (right) conditions 10 dag. (B) Primary root length of 10 dag WT and *lpr1* seedlings grown under -Pi conditions and -Pi+M conditions. (C) DAB-Perls iron staining of roots from Col-0 and *lpr1* seedlings grown under -Pi and -Pi+M conditions 10 dag.

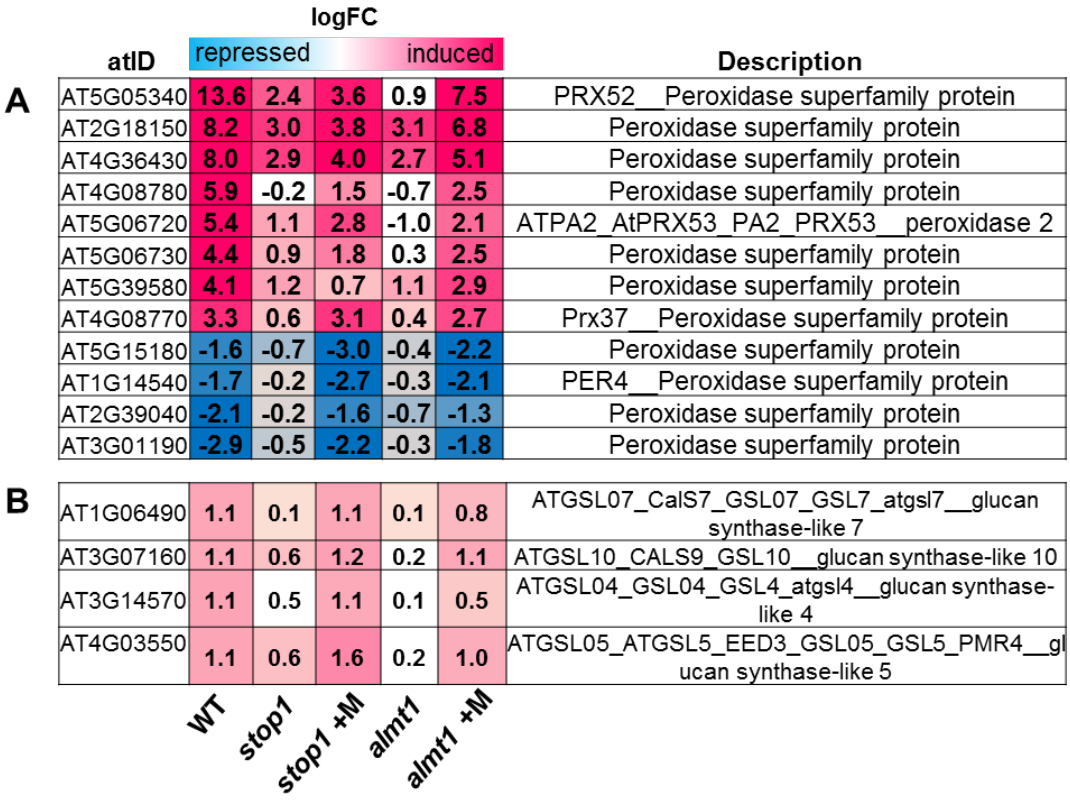

Supplementary Figure 7. **Malate treatment rescues the expression of peroxidase and callose synthase genes in Pi-deprived *stop1* and *almt1* seedlings**. The locus ID (atID), description and the expression values (logFC) of (A) *PEROXIDASE* and (B) *CALLOSE SYNTHASE* genes are presented for Pi-deprived seedlings (WT, *stop1* and *almt1*) and malate-treated Pi-deprived seedlings (*stop1*+M, *almt1*+M). Non colored values mean that the gene is not differentially expressed (FDR>.05) in the respective genotype/conditions.

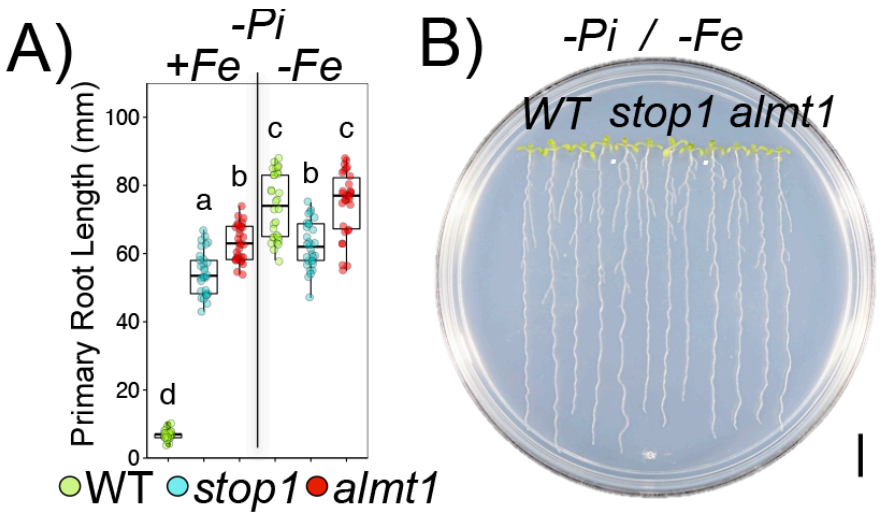

Supplementary Figure 8. Iron-dependence of the inhibition of primary root under low Pi conditions. (A) Primary root length of 10 dag WT, *stop1* and *almt1* seedlings grown In –Pi media (-Pi+Fe) and –Pi media lacking Fe (-Pi-Fe; See Materials and Methods). Green, blue and red dots depict WT, *stop1* and *almt1* individuals (n=30 from 3 independent experiments), respectively. (B) Phenotypes of 10 dag WT, *almt1* and *stop1* seedlings grown under -Pi-Fe conditions. Scale bar equals 1 centimeter (cm).

References

1. Martinez-Trujillo M, Limones-Briones V, Cabrera-Ponce JL, Herrera-Estrella L (2012) Improving transformation efficiency ofArabidopsis thaliana by modifying the floral dip method. *Plant Mol Biol Rep* 22(1):63–70.

2. Jefferson RA, Kavanagh TA, Bevan MW (1987) GUS fusions: beta-glucuronidase as a sensitive and versatile gene fusion marker in higher plants. *EMBO J* 6(13):3901–3907.

3. Malamy JE, Benfey PN (1997) Organization and cell differentiation in lateral roots of Arabidopsis thaliana. *Development* 124(1):33–44.

4. Li P, Merz KM Jr (2014) Taking into Account the Ion-induced Dipole Interaction in the Nonbonded Model of Ions. *J Chem Theory Comput* 10(1):289–297.

5. Li P, Song LF, Merz KM Jr (2015) Parameterization of highly charged metal ions using the 12-6-4 LJ-type nonbonded model in explicit water. *J Phys Chem B* 119(3):883–895.

6. Bekker H, et al. (1993) PHYSICS COMPUTING '92. *GROMACS - A PARALLEL COMPUTER FOR MOLECULAR-DYNAMICS SIMULATIONS* Available at: http://www.rug.nl/research/portal/publications/gromacs--a-parallel-computer-for-

moleculardynamics-simulations(84ef8765-003b-421d-b570-b9c5a3f78a9b).html [Accessed December 16, 2016].

7. Malde AK, et al. (2011) An Automated Force Field Topology Builder (ATB) and Repository: Version 1.0. *J Chem Theory Comput* 7(12):4026–4037.

8. Berendsen HJC, Grigera JR, P. T (1987) The Missing Term in Effective Pair Potentialst. *J Phys Chem* 91:6269–6271.

9. Bussi G, Donadio D, Parrinello M (2007) Canonical sampling through velocity rescaling. *J Chem Phys* 126(1):014101.

10. Essmann U, et al. (1998) A smooth particle mesh Ewald method. *J Chem Phys*. doi:10.1063/1.470117.

11. Darden T, York D, Pedersen L (1998) Particle mesh Ewald: An N·log(N) method for Ewald sums in large systems. *J Chem Phys*. doi:10.1063/1.464397.

12. Hess B, Bekker H, Berendsen HJC, Fraaije JGEM (1997) LINCS: A linear constraint solver for molecular simulations. *J Comput Chem* 18(12):1463–1472.

13. Parrinello M (1981) Polymorphic transitions in single crystals: A new molecular dynamics method. *J Appl Phys* 52(12):7182.

14. Barnoud J, Rossi G, Monticelli L (2014) Lipid membranes as solvents for carbon nanoparticles. *Phys Rev Lett* 112(6):068102.

15. Bolger AM, Lohse M, Usadel B (2014) Trimmomatic: a flexible trimmer for Illumina sequence data. *Bioinformatics* 30(15):2114–2120.

16. Kim D, et al. (2013) TopHat2: accurate alignment of transcriptomes in the presence of insertions, deletions and gene fusions. *Genome Biol* 14(4):R36.

17. Anders S, Pyl PT, Huber W (2015) HTSeq--a Python framework to work with high-throughput sequencing data. *Bioinformatics* 31(2):166–169.

18. Robinson MD, McCarthy DJ, Smyth GK (2010) edgeR: a Bioconductor package for differential expression analysis of digital gene expression data. *Bioinformatics* 26(1):139–140.

19. Shannon P, et al. (2003) Cytoscape: a software environment for integrated models of biomolecular interaction networks. *Genome Res* 13(11):2498–2504.

20. Bindea G, et al. (2009) ClueGO: a Cytoscape plug-in to decipher functionally grouped gene ontology and pathway annotation networks. *Bioinformatics* 25(8):1091–1093.